Experimental and Numerical Analysis of the Cellular Detonation Structure for Ethylene-Oxygen Mixtures

Ashlesh Dahake, Anil S. Karthik, S Mohamed Hussain, Ranjay K. Singh, Ajay V. Singh*
Department of Aerospace Engineering, Indian Institute of Technology Kanpur,
Kanpur-208016, U.P., India.

1 Introduction

Ethylene has garnered significant attention in recent years as a promising fuel for rotating detonation engines (RDEs) due to its favorable chemical and physical properties. Its relatively low ignition energy and fast reaction kinetics compared to other hydrocarbon fuels make it well-suited for studying high-speed combustion phenomena, including detonations. The reaction mechanisms for ethylene are well characterized, and detailed kinetic models are readily available, providing a robust foundation for both experimental and numerical investigations. Numerous experimental and numerical studies have explored C_2H_4-O_2 and C_2H_4-air RDEs [1–3]. As RDE technology advances, the transition to practical engineering applications will necessitate the use of liquid hydrocarbon fuels. Since ethylene is the primary product during the pyrolysis of higher hydrocarbon fuels such as Jet A, understanding its chemical kinetics and detonation characteristics is essential for the development of next-generation propulsion systems.

Detonation cell size is a fundamental parameter in detonation dynamics as it reflects the complex interplay between shock waves and chemical reactions. The cellular detonation structure represents the instability mechanisms driving the detonation process. The cell size is widely used as a key parameter to assess the reactivity and sensitivity of a fuel-oxidizer mixture to detonation [4]. However, cell size measurements are often limited due to experimental constraints and are subject to human interpretation. For instance, at atmospheric pressure, the cell size of ethylene-oxygen mixtures is less than 1 mm, making direct measurements from soot foils highly challenging, if not impractical. Therefore, numerical simulations have become an essential tool in detonation research, complementing experimental studies and offering deeper insights into underlying physical processes. Two-dimensional simulations based on reactive Euler or Navier-Stokes equations are widely used to capture detonation wave structures. Kailasanath et al. demonstrated the feasibility of computational fluid dynamics (CFD) for modeling detonation phenomena, paving the way for more advanced simulations [5]. Recent research has further improved the predictive accuracy by incorporating detailed chemical kinetics and multi-dimensional effects [6,7]. These simulations not only complement experimental observations but also offer predictive capabilities for conditions that are challenging to replicate in laboratory settings.

Numerical simulations have been highly successful in replicating key features of experimentally observed detonation waves, but discrepancies between simulations and experiments remain a significant challenge to date. Two-dimensional simulations effectively capture the overall cellular structure of a

*Correspondence to: ajayvs@iitk.ac.in

detonation wave, including the characteristic detonation cells and transverse waves. Additionally, trends in cell size variation with changes in mixture composition, pressure, and temperature show excellent qualitative agreement between the experimental data and numerical predictions. However, quantitative differences significantly hamper the predictive capabilities of the numerical simulations, specifically for hydrogen-based mixtures [6].

This paper presents a comprehensive analysis of the cellular detonation structure in ethylene-oxygen mixtures by integrating experimental measurements with two-dimensional numerical simulations. The study focuses on the direct comparison of the experimental and numerical detonation cellular structure. This approach not only validates the numerical model but also provides deeper insight into the underlying physical mechanisms.

2 Experimental Methodology

Detonation experiments were conducted in a 3.6 m long linear detonation tube with an inner diameter of 73 mm. The closed end of the tube featured multiple ports to accommodate a spark plug, gas feed line, vacuum pump, and a digital pressure gauge for monitoring and controlling initial test conditions. A Shchelkin spiral was installed immediately downstream of the spark plug to enhance flame acceleration and facilitate the transition to detonation. The spiral, measuring 300 mm in length with an 8 mm wire diameter and a blockage ratio of 0.3, induced turbulence to promote detonation onset. A schematic representation of the experimental setup is shown in Fig. 1. The detonation propagation velocity in the tube was measured using six high-frequency piezoelectric pressure transducers (PCB 113B24) with a sampling rate of 500 kHz. The detonation propagation velocity in the tube was evaluated based on the time of arrival data. The detonation velocity reported in the current work is the average velocity based on the five sets of measurements between adjacent transducers. The overall uncertainty in the detonation velocity measurement was less than 3%. The cellular detonation structure was experimentally captured using the soot foil technique. A minimum of 100 cell widths was measured by hand for each experiment, and each experiment was repeated twice. The measurement of cell widths in the present study encompasses a statistically significant sample size of ~ 200 cells. Further details on the experimental procedure and diagnostics can be found in our previous work [8].

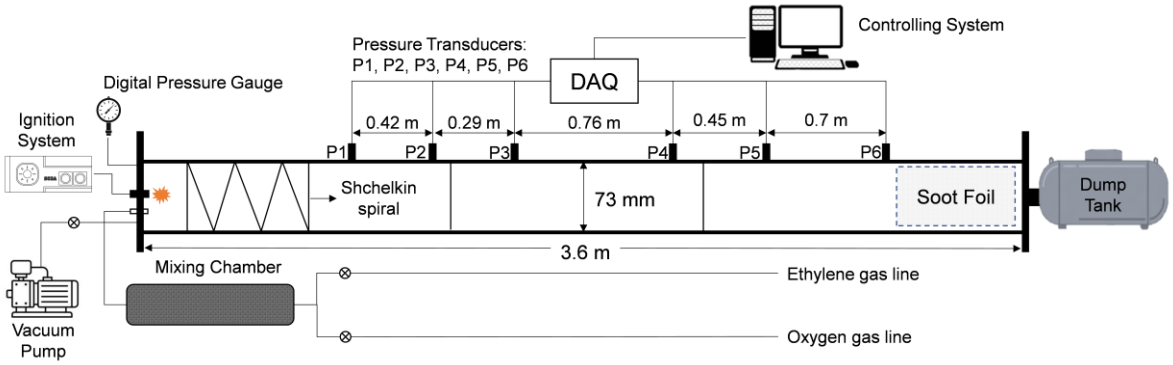

Figure 1: Schematic of the experimental setup.

3 Numerical Methodology

The compressible reactive Navier-Stokes equations were solved using DetonationFOAM [9], an OpenFOAM-based solver with dynamic meshing. The governing equations can be found in the literature elsewhere [9]. The numerical simulations employed a reduced reaction mechanism consisting of 28 species and 70 elementary reactions [10], providing an accurate representation of the complex chemical kinetics. The second-order accurate Kurganov scheme was used for shock capturing, while a central

differencing scheme was applied to discretize diffusion terms. The stiff ODE solver Implicit Seulex was employed to resolve the chemical source terms in the compressible Navier-Stokes equations. Detonation simulations were carried out using fine meshes with adaptive mesh refinement based on density gradients, allowing for a maximum refinement factor of 3 and a maximum CFL number of 0.2. A grid independence test was carried out with grid sizes of 10 µm, 5 µm, and 2.5 µm. The detonation structure and the detonation cell size showed minimal variation when the grid size was changed from 5µm to 2.5 µm. Therefore, a grid size of 5 µm was used for the computations. The computational domain is a 2D channel with a height of 4 mm and a length of 100 mm, initially filled with a stoichiometric ethylene-oxygen mixture at 298 K. The adiabatic slip wall boundary conditions were applied at the top, bottom, and inlet walls, while a zero-gradient condition was imposed at the outlet. Detonation was initiated directly through high-temperature, high-pressure hotspots at the leftmost end of the domain. The resulting local explosions and accompanying blast waves were perturbed by circular regions of fully reacted products (at elevated temperatures and pressures), accelerating the onset of cellular instabilities. Initially, the detonation was overdriven but rapidly decelerated, reaching a self-sustained velocity close to the CJ detonation velocity.

4 Results and Discussions

Detonation tube experiments and two-dimensional numerical simulations were conducted for stoichiometric C_2H_4-O_2 mixtures at 15 kPa and 25 kPa at room temperature. The detonation velocity and cell size were measured from experiments and simulations. Both the experiments and simulations were conducted well within the detonation limits, ensuring self-sustained detonation propagation.

The CJ detonation velocity was computed using the Caltech Shock and Detonation Toolbox for experimental and numerical conditions. A comparison of the experimentally and numerically measured detonation velocities is presented in Table 1. The results indicate that both the experimental and numerical detonation velocities closely match the CJ velocity under the given conditions. The ratio V/V_{CJ} for experimental and numerical cases at 15 kPa were found to be 1.014 and 0.958, respectively, confirming steady detonation propagation. Similar results were obtained for mixtures at 25 kPa. Also, since the experiments and simulations were conducted well within the detonation limits, a minimal velocity deficit was observed (refer to Table 1). Approaching the detonation limits, the chemical energy release becomes insufficient to sustain the leading shock, leading to detonation failure or transition to deflagration. However, in the present study, both experimental and numerical results confirm that the detonation waves remained well within the stable propagation regime.

Table 1: Experimental and numerical detonation parameters for stoichiometric ethylene-oxygen detonations at 15 kPa and 25 kPa. V_{CJ}, Δ_i and $E_{\mathrm{a}}/\mathrm{R}T_{\mathrm{VN}}$ were evaluated using the ZND computations.

P_0 (kPa)	V_{CJ} (m/s)	Δ_{i} (mm)	$\frac{E_{\mathrm{a}}}{\mathrm{R}T_{\mathrm{VN}}}$	Experimental				2D Simulations			
				V (m/s)	$\frac{V}{V_{\mathrm{CJ}}}$	$\bar{\lambda}$ (mm)	σ (mm)	V (m/s)	$\frac{V}{V_{\mathrm{CJ}}}$	$\bar{\lambda}$ (mm)	σ (mm)
15	2282.1	0.119	4.72	2313.7	1.0138	2.26	0.39	2185.7	0.9577	2.02	0.41
25	2306.2	0.069	4.84	2343.7	1.0163	1.43	0.31	2205.8	0.9565	1.18	0.23

The cellular detonation structure was experimentally captured using the soot foil technique, and the numerical soot foils were obtained by tracing the maximum pressure contours. The comparison between the experimental and numerical soot foils for stoichiometric C_2H_4-O_2 detonation at 25 kPa is presented in Fig. 2. The experimentally measured mean detonation cell size at 15 kPa and 25 kPa is 2.26 mm and 1.43 mm, respectively. The corresponding numerical cell sizes under similar conditions are 2.02 mm and 1.18 mm at 15 kPa and 25 kPa, respectively. The numerical cell size closely matches the experimental measurements, with discrepancies of approximately 10.62% at 15 kPa and 17.48% at 25

kPa. These differences are within an acceptable range, especially considering the subjectivity of measuring cell sizes from the experimental soot foils, where the determination of cell boundaries can be influenced by factors such as soot deposition patterns and resolution limits.

The cellular detonation structure from the experimental and numerical soot foils exhibits qualitative similarity (refer to Fig. 2). The detonation structure was observed to be irregular in the soot foils. The transverse waves in detonations with an irregular cellular structure are significantly stronger, and the mixture ignition is due to both shock compression and turbulent mixing associated with hydrodynamic instabilities. The leading shock front does not ignite the entire reactant mixture passing through it, and unburned gas pockets are formed behind the leading shock, which burn through turbulent mixing and diffusive reaction. Therefore, numerical simulations carried out using reactive Navier-Stokes equations were able to effectively capture the underlying physics. Despite the limitations of two-dimensional simulations, which do not account for the detailed chemistry and three-dimensional phenomena influencing the formation of the cellular structures, the numerical simulations still provide a good representation of the experimental cellular structure. These results confirm that high-fidelity numerical simulations can accurately predict both the detonation cell size and the cellular detonation structure. The results also highlight the potential of numerical models in complementing experimental methods, particularly when exploring detonation behavior in regimes that are difficult to replicate experimentally.

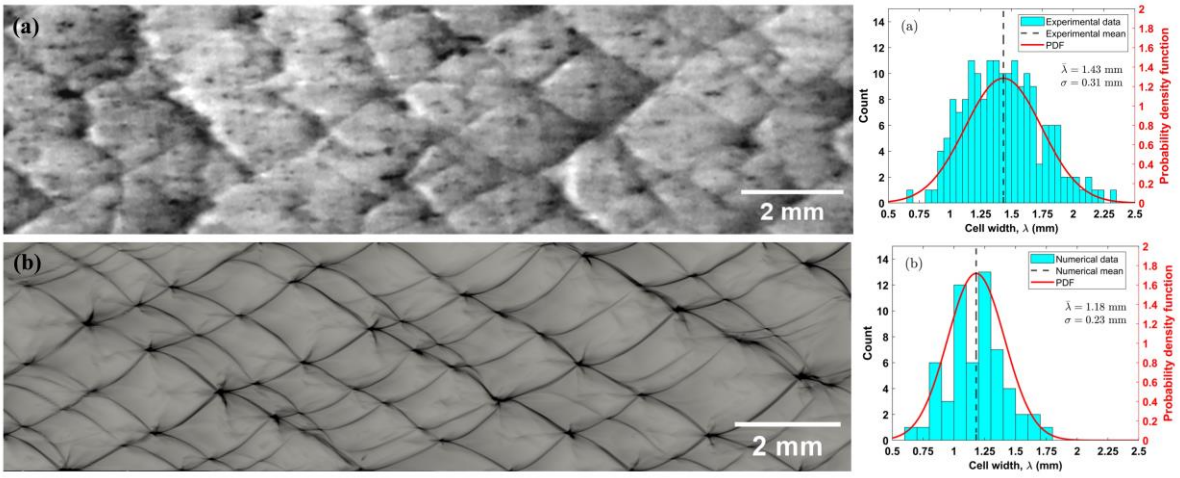

Figure 2: (a) Experimental and (b) numerical soot foils for stoichiometric ethylene-oxygen detonations at 25 kPa, along with the corresponding cell size histograms. A normal probability density function (PDF) is fitted to the cell size data (red line) to illustrate the distribution.

Previous studies highlighted significant discrepancies between experimental and numerical cell sizes, particularly in hydrogen-based detonations [6,10,11]. These studies found that numerical simulations tend to predict smaller cell sizes compared to experimental observations (~ by a factor of 2 [6]). The discrepancies have been attributed to factors such as wall energy losses and three-dimensional effects, which are often not accounted for in the simulations [10,11]. However, notable qualitative differences were observed between the regularity of experimental and numerical cell patterns in hydrogen-air mixtures [6]. Based on these observations, Taylor et al. argued that important physical processes were either neglected or inaccurately modeled in the simulations [6]. One such factor is the assumption of thermodynamic equilibrium, which is typically assumed in the simulations but may not hold over large portions of the reaction zone in a detonation wave. Thus, the observed discrepancy in cell size between the experiments and simulations for hydrogen-based mixtures was thought to be linked to the effects of vibrational nonequilibrium [6,12,13]. Taylor et al. also compared ignition delay times and vibrational relaxation times for various species in hydrogen-air mixtures [14]. Their findings indicate that the ratio of ignition delay time to vibrational relaxation time ranged from 1 to 10. Under these conditions, simulations that assume instantaneous post-shock thermal equilibrium could underestimate chemical

reaction time scales, leading to smaller predicted detonation cell sizes compared to experimental results. However, in the present study, the agreement between measured and computed cell sizes for ethylene-oxygen mixtures is excellent. This suggests that vibrational nonequilibrium does not significantly affect detonation behavior in these mixtures. To further examine this, we computed the ignition delay time and the vibrational relaxation time scales for C_2H_4 and O_2 in C_2H_4-O_2 mixtures over a range of pressures and temperatures. The vibrational relaxation times were calculated using the Millikan and White correlation [15] (Eqn. 1), following the methodology employed by Taylor et al. [14]. The vibrational relaxation time of species i in species j, τ_{i-j} is given by,

$$P\tau_{i-j} = e^{\left[A\left(T^{-\frac{1}{3}} - B\right) - 18.42\right]} \tag{1}$$

Where P is pressure (atm) and T is the temperature (K). Millikan and White also developed correlations for the parameters A and B that are quite accurate for collisions between identical or similar species. The vibrational relaxation time, τ_i of a species i, in a mixture of N gases, can be evaluated as [15],

$$\frac{1}{P\tau_i} = \sum_{j=1}^{N} \frac{X_j}{P\tau_{i-j}} \tag{2}$$

Where X_j is the mole fraction of species j and τ_{i-j} is the vibrational relaxation time of the species i infinitely diluted in species j.

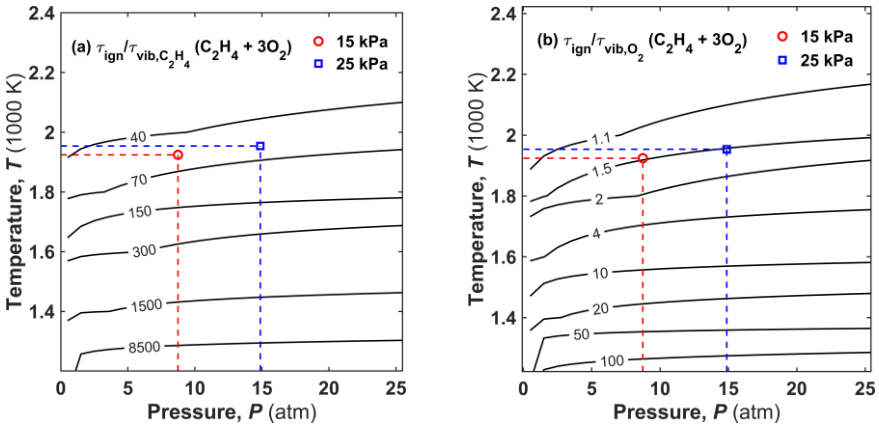

Figure 3: The ratio of ignition delay time to vibrational relaxation time for (a) C_2H_4 and (b) O_2 in the C_2H_4-$3O_2$ mixture. Both ignition delay times and vibrational relaxation times are calculated for given pressure and temperature pairs, with their ratios presented as 2D maps with iso contour lines. The hollow circle and square indicate the post-shock states for C_2H_4-O_2 mixtures at 15 kPa and 25 kPa, respectively.

The ratio of the ignition delay time (τ_{ign}) to the vibration relaxation time (τ_{vib}) of C_2H_4 and O_2 in the C_2H_4-$3O_2$ mixture is presented in Fig. 3. For each pair of temperature (T) and pressure (P), the ignition delay time was computed under adiabatic, constant-volume conditions and compared to the vibrational relaxation time of C_2H_4 and O_2. At 15 kPa, the post-shock pressure and temperature are 8.74 atm and 1924.3 K, respectively. τ_{ign}/τ_{vib} for C_2H_4 under these post-shock conditions is approximately 57, indicating that the ignition delay time is more than an order of magnitude greater than the vibrational relaxation time. Therefore, C_2H_4 molecules are vibrationally relaxed before ignition, implying that vibrational nonequilibrium effects on the ignition process are negligible for this species. However, τ_{ign}/τ_{vib} for O_2 at 15 kPa is approximately 1.4 (refer to Fig. 3b). This indicates that the ignition delay time and the vibrational relaxation time for O_2 in the C_2H_4-$3O_2$ mixture are of the same order of magnitude. Therefore, vibrational nonequilibrium in O_2 may influence the ignition process under these conditions. A similar trend is observed at 25 kPa, where the ratio τ_{ign}/τ_{vib} for C_2H_4 and O_2 was found to be ~ 56 and ~1.5, respectively. It should be noted that the Millikan and White correlation was

originally developed for diatomic species and is only accurate to within 50%. Nonetheless, it provides a reasonable first-order approximation for estimating vibrational relaxation times. Therefore, we have employed it here to qualitatively assess vibrational relaxation in ethylene-oxygen mixtures. Ethylene, being a polyatomic molecule with 12 vibrational degrees of freedom, is expected to undergo rapid vibrational relaxation [16]. The rapid vibrational relaxation of ethylene molecules is due to its extensive vibrational modes and the efficient transfer of vibrational energy through molecular collisions. The excited ethylene molecule rapidly relaxes due to the intramolecular vibrational energy redistribution among all available vibrational modes. Furthermore, ethylene acts as an effective collision partner and enhances the vibrational relaxation of O_2 through vibrational-vibrational (V–V) energy exchange, as noted by White [17]. These considerations collectively support our conclusion that vibrational nonequilibrium does not play a dominant role in ethylene–oxygen mixtures under the conditions studied.

5 Conclusions

The present work investigated the cellular structure of stoichiometric ethylene-oxygen detonations through both experiments and numerical simulations. The detonation velocities observed in both experiments and simulations closely match the CJ detonation velocity, confirming steady detonation propagation. The experimental and numerical cell sizes showed remarkable agreement, with differences of approximately 10.62% and 17.48% at 15 kPa and 25 kPa, respectively. This demonstrates the capability of high-fidelity numerical models to effectively predict detonation cell sizes and patterns under the given conditions. Additionally, the analysis of ignition delay times and vibrational relaxation times for C_2H_4 and O_2 revealed that vibrational nonequilibrium effects are less significant in C_2H_4-O_2 detonations than in hydrogen-based detonations. The computed ratio of ignition delay time to vibrational relaxation time showed that C_2H_4 molecules are vibrationally relaxed before ignition, while O_2 relaxation may influence ignition kinetics. However, the presence of C_2H_4 enhances the vibrational relaxation of O_2 through vibrational-vibrational (V–V) energy exchange. Thus, vibrational nonequilibrium is not likely to be a dominant factor in C_2H_4-O_2 detonations under the conditions studied.

Acknowledgments

The financial support from the Aeronautics Research and Development Board (ARDB) is gratefully acknowledged for the current work (Grant no. ARDB/01/1042000 M/I).

References

[1] Wang Y, Le J, Wang C, Zheng Y. *Appl. Therm. Eng.* 137 (2018), 749–57.
[2] Weijie F, Shijie L, Zhong S, Peng H, Yuan X, Liu W. *Phys. Fluids* 35 (4) (2023), 045142.
[3] Sato T, Raman V. *J. Propuls. Power* 36 (2020), 752–62.
[4] Vasil'ev AA. *J. Propuls. Power* 22 (2006), 1245–60.
[5] Kailasanath K, Oran ES, Boris JP, Young TR. *Combust. Flame* 61 (1985), 199–209.
[6] Taylor BD, Kessler DA, Gamezo VN, Oran ES. *Proc. Combust. Inst.* 34 (2013), 2009–16.
[7] Crane J, Lipkowicz JT, Shi X, Wlokas I, Kempf AM, Wang H. *Proc. Combust. Inst.* 39 (2023), 2915–23.
[8] Singh RK, Dahake A, Yadav CK, Singh AV. *Int. J. Hydrogen Energy* 80 (2024), 322–31.
[9] Sun J, Wang Y, Tian B, Chen Z. *Comput. Phys. Commun.* 292 (2023), 108859.
[10] He J, Li J, Ma X, Meng B, Tian B. *Fuel* 342 (2023), 127812.
[11] Xiao Q, Sow A, Maxwell BM, Radulescu MI. *Proc. Combust. Inst.* 38 (2021), 3641–9.
[12] Shi L, Shen H, Zhang P, Zhang D, Wen C. *Combust. Sci. Technol.* 189 (2017), 841–53.
[13] Shi X, Jayaraman AS, Wang H. *Proc. Combust. Inst.* 40 (2024), 105695.
[14] Taylor BD, Kessler DA, Oran ES. *24th ICDERS* (2013) Taipei, Taiwan.
[15] Millikan RC, White DR. *J. Chem. Phys.* 39 (1963), 3209–13.
[16] Yuan RCL, Preses JM, Flynn GW, Ronn AM. *J. Chem. Phys.* 59 (1973), 6128–35.
[17] White DR. *J. Chem. Phys.*42 (1965), 2028–32.